Modeling fracture in rate-dependent polymer networks: A quasicontinuum approach

Ahmed Ghareeb[1] and Ahmed Elbanna*[1]

[1]Department of Civil and Environmental Engineering, University of Illinois at Urbana-Champaign, Illinois, USA

May 2021

Abstract

Soft materials, such as rubber and gels, exhibit rate-dependent response where the stiffness, strength and fracture patterns depend largely on loading rates. Thus, accurate modeling of the mechanical behavior requires accounting for different sources of rate-dependence such as the intrinsic viscoelastic behavior of the polymer chains and the dynamic bond breakage and formation mechanism. In this chapter, we extend the QC approach presented in Ghareeb and Elbanna [*Journal of the Mechanics and Physics of Solids*, **137**, 103819 (2020)] to include rate-dependent behavior of polymer networks. We propose a homogenization rule for the viscous forces in the polymer chains and update the adaptive mesh refinement algorithm to account for dynamic bond breakage. Then, we use nonlinear finite element framework with predictor-corrector scheme to solve for the nodal displacements and velocities. We demonstrate the accuracy of the method by verifying it against fully discrete simulations for different examples of network structures and loading conditions. We further use the method to investigate the effects of the loading rates on the fracture characteristics of networks with different rate-dependent parameters. Finally, We discuss the implications of the extended method for multi-scale analysis of fracture in rate-dependent polymer networks.

Keywords: Quasicontinuum method, Polymer networks, Viscoelasticity

1 Introduction

Polymers constitute the major building blocks in a variety of natural and man-made materials. Structurally, polymeric materials may be abstracted as a network of cross-linked nonlinear elastic chains [1]. The topological properties of these networks, such as local connectivity, cross-linking density, and bond types, may dramatically affect their mechanical response and fracture proprieties [2, 3]. Deformation and damage on the network micro scale is usually inaccessible to direct experimental measurements and visualization, thus, the relation between the material topology and mechanical response of these materials remains elusive. Multiscale numerical models are thus needed to bridge this gap [2].

Modeling of soft polymeric materials has been mainly approached using continuum theories, including linear elasticity, hyperelasticity, viscoelasticity, viscoplasticity and poroelasticity [4, 5, 6, 7, 8]. While these techniques enabled significant progress in modeling the elasticity and distributed damage behavior of polymeric materials, continuum descriptions are usually independent of the size scale of the network structures and may not capture localized phenomena without enrichment [**?**], which in many cases is either expensive or is based on idealized models of microstructure. In particular, when it comes to fracture, a phenomenon that depends critically on the local conditions in the vicinity of the propagating cracks, continuum methods are not suited for predicting the effect of the network local topology on its fracture resistance [3].

*Corresponding author: Ahmed Elbanna, elbanna2@illinois.edu

Recent advances in imaging, computational power, and nano/micro fabrication technologies have led to the need of modeling fundamental material behavior starting from the atomic scale [9]. For the accurate representation of the material response at this scale, the material must be modeled using discrete simulations. Discrete simulations have been widely used to model polymeric materials as networks of irregular lattices with different link models that incorporate the polymer chain physics [10]. Adapting these discrete models where each polymer chain is modeled explicitly, it is possible to accurately describe localized phenomena such as fracture and cavitation. However, discrete simulations are usually limited to small scale samples due to the computational challenges associated with the large number of degrees of freedom.

Recently, We have introduced a new adaptive numerical algorithm for modeling fracture in polymer networks using an extended version of the Quasi-Continuum method [11, 12, 13] that accounts for both the nonlinear elastic nature of the polymer chains as well as the geometric nonlinearity associated with their potentially large deformation [14]. In regions of high interest where deformation gradients are non uniform, for example near crack tips, explicit representation of the local topology is retained where each polymer chain is idealized using the worm like chain model. Away from these imperfections where the deformation gradient is sufficiently uniform, the network structure is computationally homogenized, using an equivalence of the microscale and macroscale incremental work, to yield an anisotropic material tensor consistent with the underlying network structure. Thus at any instant in time, only a fraction of the network nodes is solved. Dynamic adaptivity allows efficient transition between the two resolutions. This approach enables modeling crack propagation without apriori constraint on the fracture energy or the need to assume phenomenological length scales, while maintaining the influence of large-scale elastic loading in the bulk.

Soft materials, such as rubber and gels, exhibit rate-dependent response where the stiffness, strength and fracture patterns depend largely on loading rates. Rate-dependence in polymer networks emerge from different sources such as intrinsic viscoelasticity in the polymer chain behavior, dynamic bond breakage, or viscous drag between polymer network and infused fluids. In a previous study [3], discrete polymer networks were modeled considering the rate-dependent response emerging from two major contributions: (1) breakage and formation of end bonds and cross-linkers, and (2) viscous drag arising from the relative motion of the deforming polymer network and infused fluids. Extensive research has also been done previously for experimental characterization of the elastic and loss mdodulii [15, 16]. Continuum models based on phenomenological as well as homogenization approaches also exist which have been successful in predicting effective elastic and viscoelastic properties [17, 18, 19].

In this Study, we extend on the QC approach to account for different sources of rate-dependence in the polymer networks. In the current study, we add viscoelasticity to the polymer chain behavior through kelvin-Voigt model and derive a novel homogenization rule for the QC implementation. We also take into consideration the dynamic bond breakage where the bond failure depends on the polymer stretch rate. This paper is organized as follows. In Section 2, we introduce the homogenization technique for the extended QC, then we present the polymer chain constitutive law, and the dynamic bond breakage governing equations. The numerical implementation algorithms used in this study are presented in Section 3. We verify the numerical algorithm for modeling loading/unloading of pristine samples and damage of 2D polymer networks in Section 4. In Section 5, we demonstrate the efficiency of the method by applying it to study the fracture of polymer networks with different rate-dependence parameters. We show the effects of polymer chain viscoelasticity, dynamic bond breakage, and loading rates on the failure patterns of 2D notched samples. Finally, We discuss the method implications for the analysis of networked material systems in Section 6.

2 Quasicontinuum method formulation for Irregular Viscoelastic Polymer Networks

2.1 Micro to macro scale homogenization: Viscoelasticity

To model the viscoelasticity on the chain level, a simple Kelvin-Voigt model is adapted where each link is modeled as a purely nonlinear elastic spring, defined by the worm-like polymer chain model, and a purely viscous damper connected in parallel, the model is shown in Fig.1. The viscous

damper is defined by a viscosity parameter η_p that can be pre-specified as a constant value, a function of time, or a function of stretch. The total force in each link is given by:

$$f = f^e + f^v \tag{1}$$

Where f is the total force, f^e is the elastic force given by the force-stretch behavior of the spring, and f^v is he viscoelastic force which is a function of the damper viscosity parameter and the stretch rate.

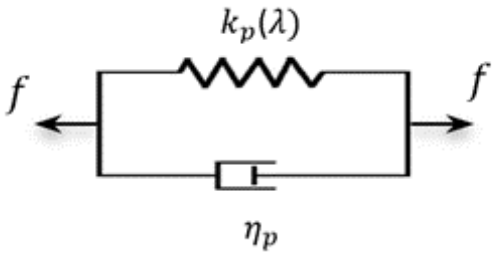

Figure 1: The Kelvin-Voigt viscoelastic model for a polymer chain: The link is modeled as a spring defined by the worm-like chain force-extension relation in parallel to a viscous damper defined by a viscosity parameter η_p.

To map the microscopic behavior on the macroscale, a homogenization rule is required. We establish the micro-macro scale transition relation based on the Hill-Mandel condition [20, 21]. This condition requires the volume average of the variation of work on the micro level to be equal to the variation of local work on the macroscale:

$$\delta W_{Macro} = \delta W_{micro} \tag{2}$$

We have derived the homogenization rule for elastic networks in Ghareeb and Elbanna [22]. The 2^{nd} Piola-Kirchhoff Stress tensor and the corresponding elasticity tensor are given by:

$$S^e_{ij} = \frac{1}{V_o}\sum_{p=1}^{N_p}\left(F^{p\ -1}_{ik} f^{ep}_{k} L^p_j\right) \tag{3}$$

$$C^{S^eE}_{ijkl} = \frac{1}{V_o}\sum_{p=1}^{N_p}\left(L_j F^{-1}_{im}\frac{\partial f^e{}_m}{\partial l_n} F^{-1}_{kn} L_l\right) - F^{-1}_{in} F^{-1}_{ln} S^e_{jk} \tag{4}$$

Here, we derive the homogenization rule for the viscoelasticity case following the same procedure for homogenization of the purely elastic model detailed in [22]. The full derivation is given in Appendix A. The homogenized viscoelastic stress and modulus are thus given by:

$$\mathbf{P}^v_M = \frac{1}{V_o}\sum_{p=1}^{N_p}\vec{f}^v_p \otimes \vec{L}_P = \frac{1}{V_o}\sum_{p=1}^{N_p} f^v_p L_p \vec{n}_p \otimes \vec{N}_p \tag{5}$$

$$\mathbf{C}^{\mathbf{P}^v\dot{\mathbf{F}}} = \frac{1}{V_o}\sum_{p=1}^{N_p}\vec{L}_P \otimes \eta_p \otimes \vec{L}_P = \frac{1}{V_o}\sum_{p=1}^{N_p}\eta_p L^2_p \vec{N}_P \otimes \vec{n}_P \otimes \vec{N}_P \otimes \vec{n}_P \tag{6}$$

For computational purposes, we chose to use the symmetric quantities to assemble the tensors. The quantities are given by:

$$S^v_{ij} = \frac{1}{V_o}\sum_{p=1}^{N_p}\left(F^{p\ -1}_{ik} f^{vp}_{k} L^p_j\right) \tag{7}$$

$$C^{S^v\dot{E}}_{ijkl} = \frac{1}{V_o}\sum_{p=1}^{N_p}\left(L_j F^{-1}_{im}\frac{\partial f^v{}_m}{\partial V_n} F^{-1}_{kn} L_l\right) - F^{-1}_{in} F^{-1}_{ln} S^v_{jk} \tag{8}$$

2.2 Assembling the tensors

Since the links in the network have axial deformations only, the deformation gradient and its inverse for each link can be written as:

$$F_{ij} = \lambda n_i N_j \tag{9}$$

$$F^{-1}_{ij} = \frac{1}{\lambda} N_i n_j \tag{10}$$

Where $\lambda = l/L$ is the stretch, n_i is the unit vector in the current configuration, and N_i is the unit vector in the original configuration.

The elastic and viscoelastic PK2 stress tensors are given by:

$$S^e_{ij} = \frac{1}{V_o} \sum_{p=1}^{N_p} \left(\frac{1}{\lambda} f^e L \right) N_i N_j \tag{11}$$

$$S^v_{ij} = \frac{1}{V_o} \sum_{p=1}^{N_p} \left(\frac{1}{\lambda} f^v L \right) N_i N_j \tag{12}$$

Whereas the elastic material and viscoelastic modulus tensors are given by:

$$C^{S^e E}_{ijkl} = \frac{1}{V_o} \sum_{p=1}^{N_p} \left(\frac{1}{\lambda^2} k L^2 - \frac{1}{\lambda^3} f^e L \right) N_i N_j N_k N_l \tag{13}$$

$$C^{S^v \dot{E}}_{ijkl} = \frac{1}{V_o} \sum_{p=1}^{N_p} \left(\frac{1}{\lambda^2} \eta L^2 - \frac{1}{\lambda^3} f^v L \right) N_i N_j N_k N_l \tag{14}$$

Here $k = \partial f^e / \partial l$ and $\eta = \partial f^v / \partial \dot{l}$ are the link tangent stiffness and viscosity, respectively, where f^e, f^v and L are the magnitudes of the link elastic force, viscoelastic force and reference length respectively. The stress tensors $\mathbf{S}^e$ and $\mathbf{S}^v$ are symmetric, and the tensors $\mathbf{C}^{S^e E}$ and $\mathbf{C}^{S^v \dot{E}}$ both have major and minor symmetries.

2.3 Polymer chain constitutive law

We use the same polymer chain constitutive model used in Ghareeb and Elbanna [22] where each link in the polymer network is modeled using a nonlinear elastic force elongation relation give by the worm like chain model. The force-elongation relation and the chain stiffness are given by [23]:

$$f^e = \frac{k_B T}{b} \left[\frac{1}{4} \left(1 - \frac{x}{L_c} \right)^{-2} - \frac{1}{4} + \frac{x}{L_c} \right] \tag{15}$$

$$k = df/dx = \frac{k_B T}{b} \left[\frac{1}{2 L_c} \left(1 - \frac{x}{L_c} \right)^{-3} + \frac{1}{L_c} \right] \tag{16}$$

Where f is the force, x is the end-to-end distance, b is the persistence length, k_B is Boltzmann' constant, T is the temperature, and L_c is the contour length of the polymer chain. We assume the network is force balanced at the reference configuration.

These expressions are used to compute the homogenized stress and elasticity tensor. As the end-to-end distance x approaches the contour length L_c, the polymer chain response becomes highly nonlinear as both the force and the stiffness values go to infinity. This signals a limitation of this constitutive description which may be circumvented by accounting for strain energy of the chain in addition to its entropic energy [24]. Such correction will be investigated further in future work. In this study, such extreme limit is not probed as the chains will fail prior to that as will be discussed in the next section.

In addition, we assume each polymer chain exhibits a viscoelastic behavior modeled by a Kelvin-Voigt model. The viscoelastic force is given by:

$$f^v = \eta\left(\frac{\dot{x}}{L_c}\right) \tag{17}$$

Where η is the viscoelasticity parameter that can be pre-specified as a constant value, a function of time, or a function of stretch, and $\left(\frac{\dot{x}}{L_c}\right)$ is the stretch rate.

These constitutive equations are used in Eq.11, Eq.12, Eq.13 and Eq.14 to compute the homogenized elastic and viscoelastic stress, as well as the elasticity and the viscoelastic modulus tensors. In this study, we consider two different failure criteria for the polymer chains. The first is maximum stretch failure criterion, where we assume the link would fail if its stretch relative to the available contour length $\lambda_p = l/L_c$ exceeds a threshold value that is predefined. This failure criterion is appropriate for networks without transient bonds. In addition, we consider a failure criterion, for networks with transient bonds, based on transition state theory for bond breakage [25] as discussed in the next section.

2.4 Dynamic bond breakage

In this study, we consider the breakage of the bond between the polymer and the cross-linking molecule. This process is rate-dependent and is controlled by the force in stretched polymer chains at the cross-linker nodes. We assume that the breakage of polymer network bonds follows a two-state pathway where the bond is assumed to have a double-well potential with two stable states that correspond to the two energy minima in this potential: an intact state and a dissociated state. The transition reaction between the intact and dissociated states is facilitated by activation over an energy barrier which corresponds to the transitional intermediate local maximum in the energy potential shown in Fig.2. We define the rates of the forward reaction, k_f (bond formation) and backward reaction, k_b (bond breakage) that depend on the force applied by the polymer chain on the cross-linker polymer junction [3].

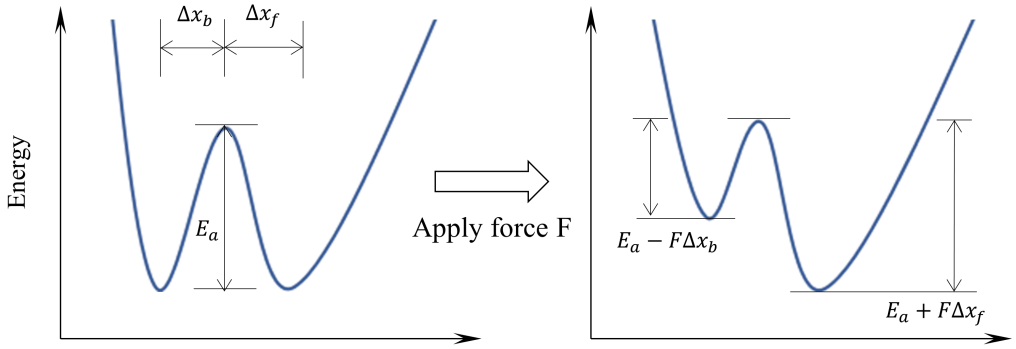

Figure 2: Schematic of the transition state theory where applying external force decreases the required energy for forward reaction and increases the same for the backward reaction, favoring bond breakage [3].

Following Bell's theory [26], the rates of bond formation and breakage are given by:

$$k_b = \alpha_b \exp(\frac{F\Delta x_b}{K_B T}) \quad , \quad k_f = \alpha_f \exp(\frac{-F\Delta x_f}{K_B T}) \tag{18}$$

Where Δx_b and Δx_f are the distances to the transition states and α_b and α_f are the inverse time scales describe the rate at which bond breakage and formation events occur at zero pulling force. Both of these parameters are assumed to be constant in this study. At large forces and pulling rates, the formation of bonds can be neglected and only bond breakage is considered [25].

We assign a binary variable, $N \in \{0, 1\}$ for each link present in the network. $N = 0$ would represent the cross-linker connection is broken and $N = 1$ indicates that this bond is intact. A

bond breakage event occurs when N_b decreases by unity, that is, when N_b^* reaches an integer [25]. Thus the condition for a bond breakage event to happen is:

$$\int dN_b^* = \int (-k_b N_f + k_f N_b) dt = -1 \tag{19}$$

where the integral on the right-hand side is over the time between successive bond breakage events. We define:

$$\delta = \int_0^{\Delta t} \frac{dn}{dt} dt \tag{20}$$

This equation is calculated for each link, and a bond is considered broken when $\delta \leq -1$.

3 Numerical Implementation

To couple the micro and macro-scales, the network nodal displacements u_n and velocities $\dot{u}_n$ are related to the representative nodes (repnodes) displacement u_R and velocities $\dot{u}_R$ through the interpolation functions:

$$u_n = \sum_{i=1}^{N_{rep}} \phi_R u_R \tag{21}$$

And

$$\dot{u}_n = \sum_{i=1}^{N_{rep}} \phi_R \dot{u}_R \tag{22}$$

where ϕ_R is the interpolation function associated with repnode R, and N_{rep} is the number of repnodes. Using the compact support of the finite element shape functions, the displacement and velocity of each node is determined from the sum over the three vertices of the triangle containing this node. Here, we use linear shape functions which turns out to perform satisfactorily [22].

After evaluating the network nodal displacements and velocities, the stress and material tangent tensors are assembled as shown in Algorithm 1.

Algorithm 1: Homogenization of QC elements

```
Calculate the network nodal displacements and velocities from the last QC solution
  through interpolation functions given in Eq.21 and Eq.22;
for each QC element Ω_i do
    for each link inside element Ω_i do
        calculate link forces f^e and f^v v from Eq.15 and Eq.17 respectively;
        calculate link stiffness k from Eq.16;
        calculate link stretch λ = l/L;
        update S^e and S^v using Eq.11 and Eq.12 respectively;
        update C^{SE} and C^{S^v Ė} using Eq.13 and Eq.14 respectively;
    end
end
```

Since we use the total Lagrangian formulation, the reference configuration quantities, such as the reference length L, and the reference unit vector N, are calculated at the system initialization and are stored instead of calculating them each time step. This leads to further computational savings. While QC methodologies normally use two reduction steps: limiting the degrees of freedom to a small fraction of the nodes and sampling of the lattice interactions for efficient energy summation [27, 28], in the current work, due to the network irregularity, we account for the contribution of all links in each continuum element in the homogenization procedure [29]. We discuss possible alternative approaches in Section 6.

3.1 Automatic mesh adaptivity

Automatic mesh adaptivity is a critical ingredient for the efficient implementation of the QC method as it enables the QC mesh to evolve dynamically based on the crack propagation path. In our proposed approach, we mark a 2D finite element Ω_i for refinement if it meets one of the following criteria:

1. Link stretch criterion:
$$\lambda_p > \lambda_{th} \quad p \in \Omega_i \tag{23}$$
Where $\lambda_p = l/L_c$ is the stretch relative to the polymer chain contour length of any network link inside the QC element Ω_i, and λ_{th} is a threshold value. The threshold value is chosen as a fraction of the failure stretch. Instead of checking this criterion for each link inside the element, we calculate the maximum principal stretch for each continuum element and check this value against the threshold:
$$\lambda_{max} = \sqrt{Max(Eig(\mathbf{F}^T\mathbf{F}))} \tag{24}$$

2. Dynamic bond breakage criterion:
$$\delta \leq -1 * \alpha_{th} \tag{25}$$
Where δ is calculated from Eq.20 using the force resulting from the maximum principal stretch calculated from Eq.24, and α_{th} in a reduction factor set to be 0.85 to account for irregularity in network topology.

3. Deformation gradient error criterion [12]:
$$\varepsilon_i = \left(\frac{1}{V_{\Omega_i}} \int_{\Omega_i} (\bar{\mathbf{F}} - \mathbf{F}_i) : (\bar{\mathbf{F}} - \mathbf{F}_i) dV \right)^{\frac{1}{2}} > \varepsilon_{th} \tag{26}$$
Where ε_i is a scalar measure that quantifies the error introduced into the solution by the current density of representative nodes, V_{Ω_i} is the volume of element Ω_i, $\mathbf{F}_i$ is the QC solution for the deformation gradient in element Ω_i, $\bar{\mathbf{F}}$ is the L_2-projection of the QC solution for $\mathbf{F}$ given by $\bar{\mathbf{F}} = \phi \mathbf{F}_{avg}$ where ϕ is the shape function array, and $\mathbf{F}_{avg}$ is computed by averaging the deformation gradient in each element sharing a given repnode, and ε_{th} is a specified threshold value.

We use the same refinement algorithm used in Ghareeb and Elbanna (2020) [22] which is based on the the standard Rivera algorithm [30].

3.2 Time adaptivity

Time adaptivity is required for computational efficiency by allowing larger time steps, when possible, without compromising accuracy. Time adaptivity is also critical for the accurate modeling of fracture in high interest zones where small time steps are needed to accurately resolve crack propagation. Using a constant time step may be overly restrictive if a small time step is used throughout and may lead to inaccurate results if a large time step is perpetually maintained. Time adaptivity balances computational cost and error.

The simulation starts with a stable large time step, that accurately and efficiently compute the nonlinear elastic deformation. The algorithm has two time refinement criteria which are usually triggered when the discrete elements approach failure, either by link stretch or dynamic bond breakage. The first refinement criterion is to ensure convergence where the time step is reduced, if needed, to reach the stable time step required for the solution convergence. The second criterion is to ensure accuracy in predicting the crack propagation as large time steps may lead to overestimating the number of failed links. Once failure initiates, the time step is reduced progressively such that further reduction in the step size has a minor affect on the number of elements failing at the current time step. This criterion also makes sure that the time step is limited by the value required for integrating the dynamic bond equations.

3.3 Nonlinear finite element framework

We use a nonlinear finite element framework to solve for the system quasi-dynamic equilibrium neglecting the inertial effects. We use a predictor-corrector scheme to solve the equation:

$$\widetilde{K}u + C\dot{u} = F \tag{27}$$

Where $\widetilde{K}$ is the assembled stiffness matrix, C is the equivalent damping matrix, F is the force vector u and $\dot{u}$ are the nodal displacement and velocity. The algorithm used for adaptive modeling of fracture in polymer networks is detailed in Algorithm 2. The homogenization is performed on the fly to provide the stress and the material tangent tensor each time step.

Algorithm 2: Adaptive QC based finite element framework

```
Initialize the system, construct the initial mesh with required information;
for step = 1,2,.....,n do
    Calculate the homogenized material consistent tangent, the viscoelastic modulus tensor
     and the elastic and viscoelastic stress tensors using Algorithm (1);
    Apply the step incremental boundary conditions at step n;
    Assemble the system internal elastic and viscoelastic force vectors, the tangent matrix,
     and the equivalent damping matrix;
    Use a predictor-corrector scheme to solve for the nodal displacement and velocities;
    For each 2D element check the mesh adaptivity conditions, add all elements marked for
     refinement to a set E_ref;
    if E_ref is not empty then
        Refine the current mesh, update system information;
        Repeat the current time step to balance the new mesh system;
    else
        Store the relevant outputs for the current time step;
        Proceed to the next time step;
    end
end
```

3.4 Disorder in polymer networks

We introduce non-uniformity in the polymer networks in two ways. First, we shift the position of the network nodes randomly with respect to a reference perfectly ordered lattice. The maximum shift values in x and y directions are $\mu_g L_x$ and $\mu_g L_y$, respectively, where μ_g is the geometric nonconformity parameter. Second, we draw the polymer chain contour length L_c randomly from a uniform distribution ranging between $[(1-\mu)L_c, (1+\mu)L_c]$, where μ is the contour length nonconformity parameter. Changing L_c affects the link force and stiffness as per Eq.15 and Eq.16. Finally, in this study we assume the viscous damper parameter η_p follows the same stochastic distribution as the polymer chain contour length.

4 Verification

For verification of the proposed methodology, we run multiple tests for both pristine and cracked samples with different parameters. In each case, we verify the QC results by comparing it to the results of the fully discrete model. We define the normalized force as fb/k_BT (Eq.15), and we normalize the viscoelastic parameter η by the initial stiffness of the polymer chain k_o.

4.1 Loading/Unloading of polymer networks

The homogenization scheme was verified by comparing the discrete and QC results of a pristine sample subjected to tension (Fig.3-a) and tension+shear (Fig.3-b). The pristine sample has dimensions of 64x64 units. The boundary conditions are such that the bottom edge is restrained

from movement in both directions and the top edge is clamped and is pulled vertically for the case of tension, or vertically and horizontally in the case of tension combined with shear. The QC mesh is refined at the edges where higher errors are expected [22]. The non zero intercepts at (Fig.3-a) and tension+shear (Fig.3-b) result from the non-zero loading rate at the start and end. These would diminish through gradual application of the load.

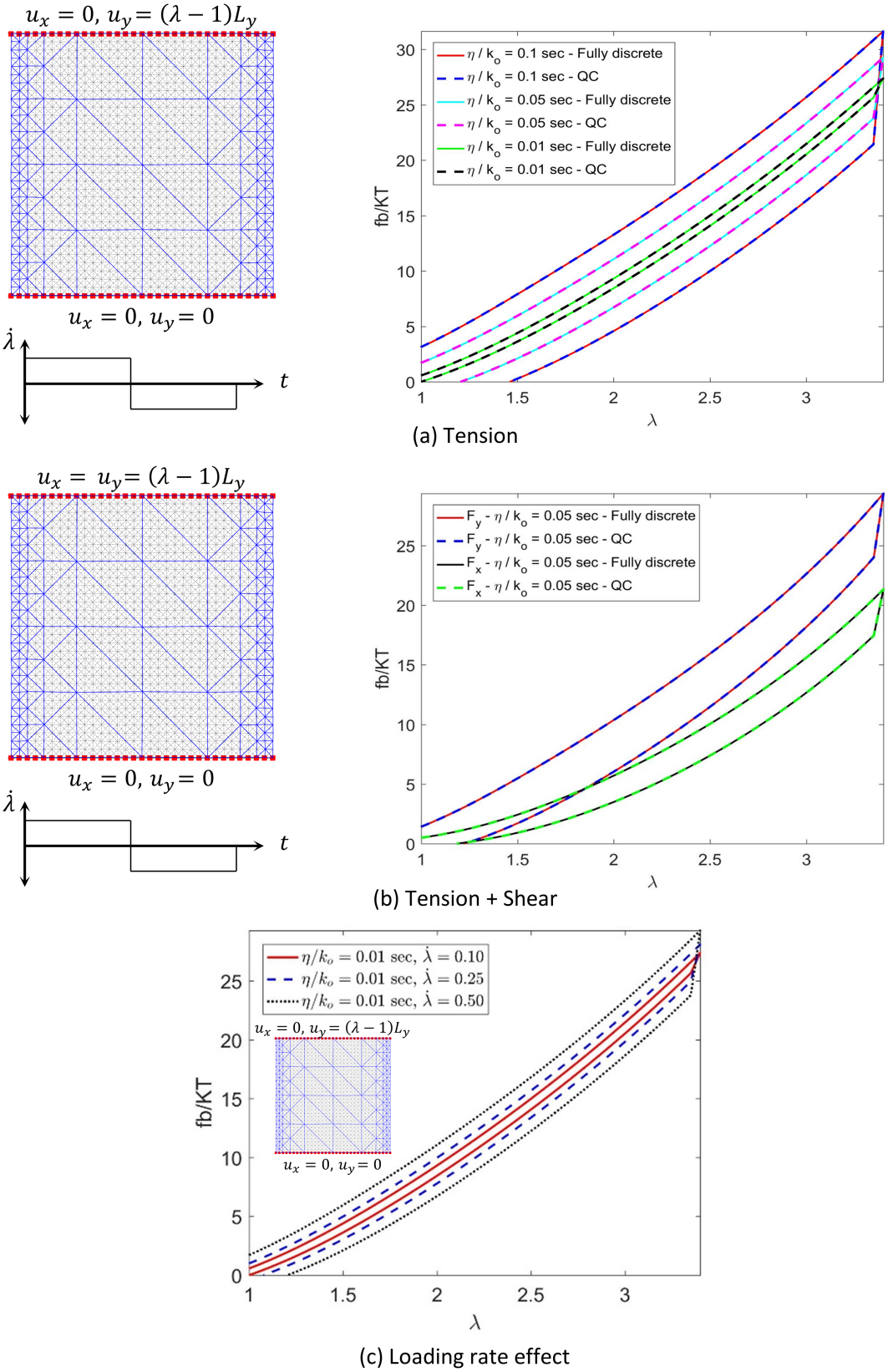

Figure 3: Verification of the QC approach with viscoelasticity applied to pristine networks. Panels (a)and (b) show networks under tensile loading, and combined tensile and shear loading. The network and the QC mesh with the applied boundary conditions are shown along with both the fully discrete and the QC approach results for different values of η/k_o values. Whereas Panel (c) shows the effect of changing the load rate on the QC force stretch relation.

The verification results in Fig.3-a,b show that the QC method capture the behavior nearly exactly for the networks considered here under tension and tension combined with shear loading conditions. Furthermore, the results from the QC model show the expected rate-dependence trends. Peak force and hysteresis increase as the loading rate increases as seen in Fig.3-c. The area enclosed between the loading and unloading branches represents the viscous energy dissipated.

4.2 Creep-recovery response

The verification results in Fig.4 also show that the QC method capture creep recovery response of pristine polymer networks subjected to a step tensile stress at the upper edge while constrained in the vertical and horizontal directions on the lower edge. Once the stress is removed, the deformations are recovered and the relaxation time depends on the normalized viscosity parameter η/k_o. Fig.4 shows that there is a near exact match between the fully discrete and the QC results.

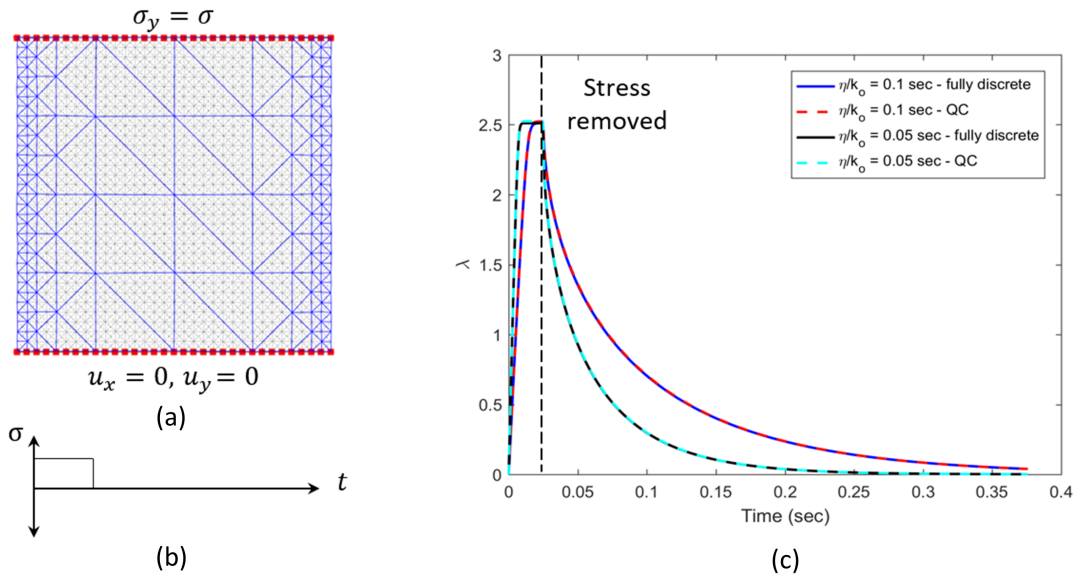

Figure 4: Creep-Recovery Response of pristine polymer networks with Kelvin viscoelasticity model: (a) The network and the QC mesh, (b) the applied stress, and (c) stretch vs. time from both discrete and QC results for 2 different normalized viscosity parameters η/k_o values.

4.3 Rate-dependent failure

Here, we model crack propagation in a notched network using both fully discrete and QC models with dynamic bond breakage at different stretch rates. The chain length is drawn from a uniform random distribution with $\mu = 0.05$. Automatic mesh adaptivty is turned on to allow the high interest area to evolve with the crack propagation. The network has dimensions of 128x64 units and the parameters for the dynamic bond breakage are $\Delta x_f = 0.25nm$, $\Delta x_b = 0.10nm$. $\alpha_b = 0.1s^{-1}$, and $\alpha_f = 0.3s^{-1}$ as per [25]. The force vs. stretch relation for both cases are shown in Fig.5. Fig.5 shows that the errors in the force stretch behavior is less than 1% for both rates. In this case, the first QC mesh has a repnodes ratio of only 2.25%, whereas the final mesh has 9.2% repnodes ratio. The significant reduction in the number of degrees of freedom lead to more than one order of magnitude reduction in computational time. These results verify that the proposed QC method can capture the dynamic bond breakage response at a fraction of the cost of the fully discrete model.

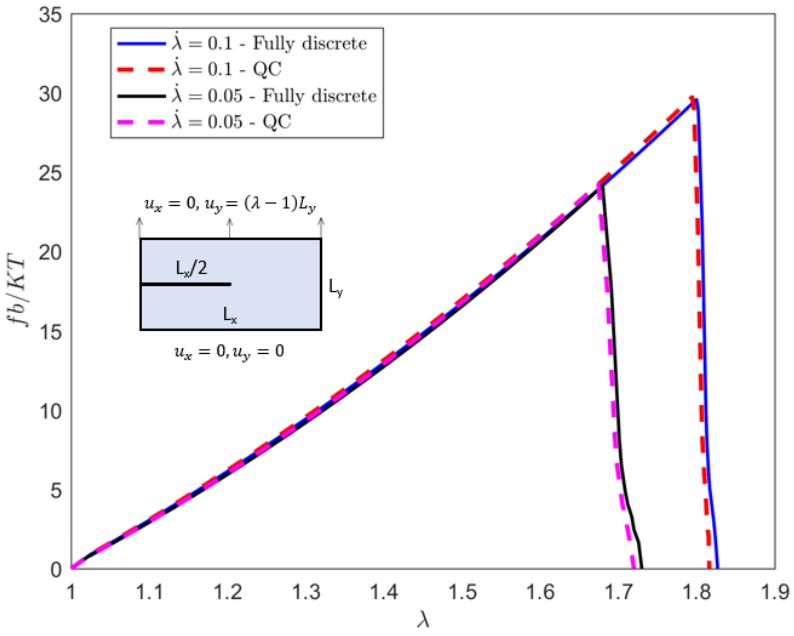

Figure 5: Verification of the QC method with dynamic bond breakage for a fracture test: The normalized force vs. stretch from QC and discrete results at two different stretch rates. The insert shows the geometry of the sample.

5 Results: Rate-dependence in Polymer Networks

In this section, we apply the QC method to investigate the rate-dependence effects on the network mechanical properties and its fracture characteristics. We consider rate-dependence due to viscoelasticity in the polymer chain constitutive law and the dynamic bond breakage failure. We show the advantage of the QC method in accurately resolving damage and fracture without the need to explicitly model every node of the network. As explained earlier, the discrete representation is limited to the zone around the crack or damage zones, and evolves with the evolution of these inhomogeneities, whereas the regions away from cracks and damage are homogenized consistently. This introduces a computationally efficient and accurate representation of the fracture process.

5.1 Polymer chains with covalent bonding (no dynamic bonds)

Fig.6-a shows the force stretch response of polymer networks at three different stretch rates. The polymer chains are assumed to have linear viscoelastic behavior that follows Kelvin-Voigt model with maximum stretch damage criterion. Fig.6-a shows that as the stretching rate increases for the strain rates considered here, the normalized peak force, the peaks stretch, and the total area under the curve increases. Furthermore, Fig.6-b,c show that the normalized peak force and the normalized energy (defined as total area under the force vs. stretch curve) scales with the stretching rate. The peak force increases almost linearly with increasing the stretch rate, while the energy dissipation increases at a nonlinear rate.

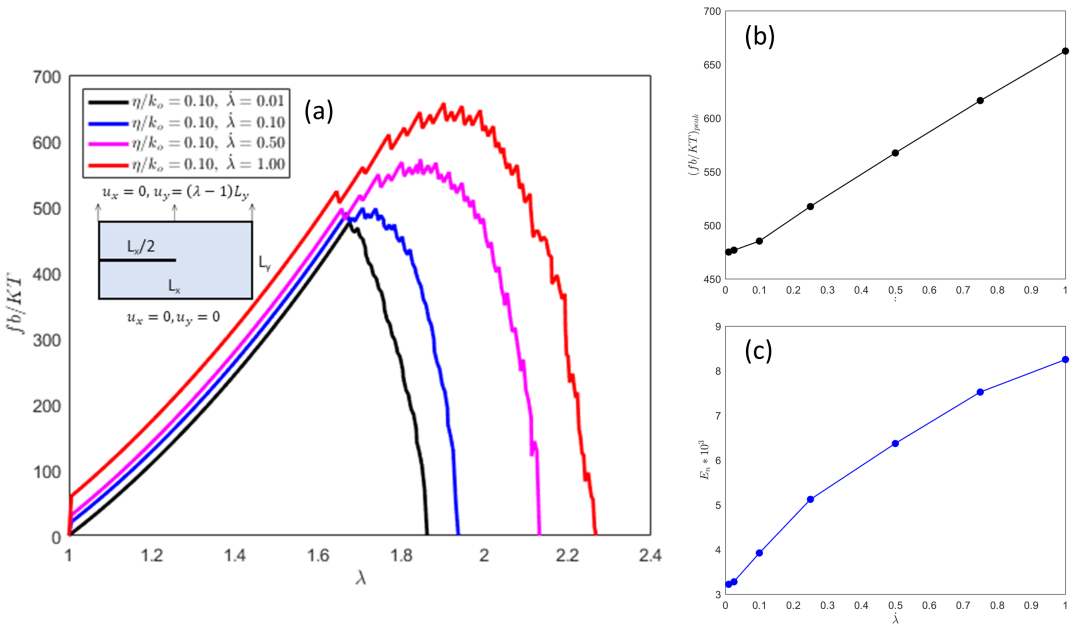

Figure 6: Fracture of networks with viscoelastic link behavior and maximum link stretch damage criterion: (a) the force vs. stretch for three different stretch rates, the network geometry and boundary conditions are shown in the insert, (b) the peak force vs. stretch rate, and (c) the total energy vs. stretch rates. The figure shows that both peak force and energy scale with the stretching rate.

5.2 Polymer chains with dynamic bonding (no viscoelasticity)

Fig.7-a shows the force stretch response of polymer networks with dynamic bond breakage damage criterion at three different stretch rates. The polymer chains are assumed to be without any viscoelastic behavior. Fig.7-a shows that as the stretching rate increases, the peak force, the peak stretch, and the total area under the curve increases. Furthermore, Fig.7-b,c show that the peak force and energy scale with the logarithmic of the stretch rate. These results are consistent with the transition dynamics of the bonds and agree with the reported results in the literature for smaller scale networks using a fully discrete approach [3].

5.3 Viscoelastic polymer networks with dynamic bonding

In this section, we investigate the combined effects of viscoelastic polymer chain response, dynamic bond breakage, and stretching rate on the failure patterns of polymer networks with a notch. The phase diagram in Fig.8 qualitatively shows the 4 different fracture patterns observed: Crack blunting and bulk damage, steady state crack propagation, crack arrest, and non steady state crack propagation. The inserts show examples of failure patterns in each case.

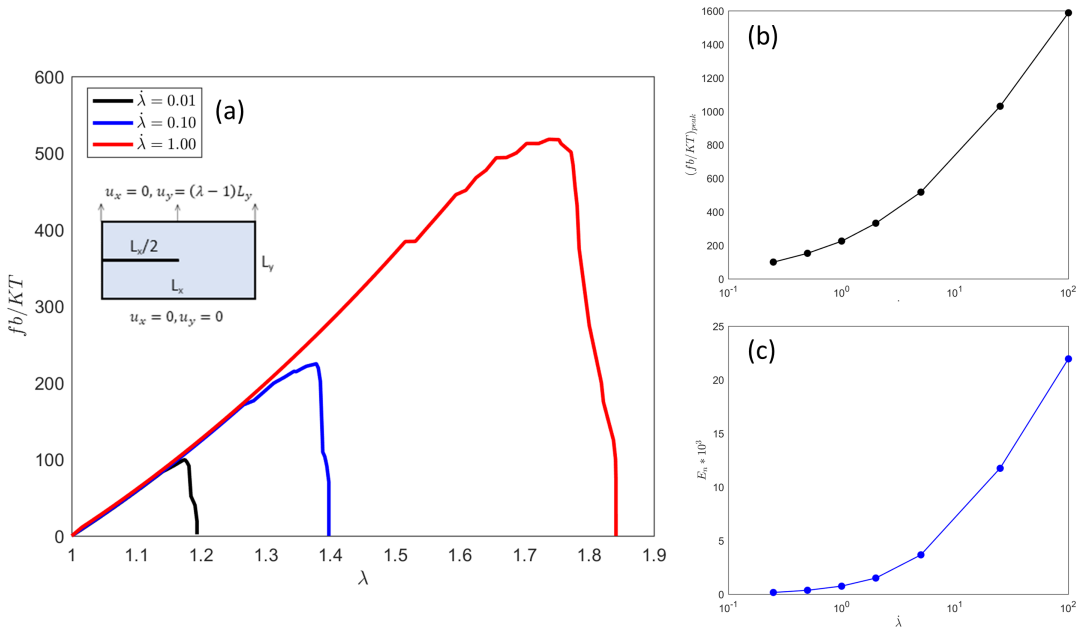

Figure 7: Fracture of networks with dynamic bond breakage failure criterion: (a) the force vs. stretch for three different stretch rates, the network geometry and boundary conditions are shown in the insert, (b) the peak force vs. stretch rate, and (c) the total energy vs. stretch rates. The figure shows that both peak force and energy scale with the log of the stretching rate.

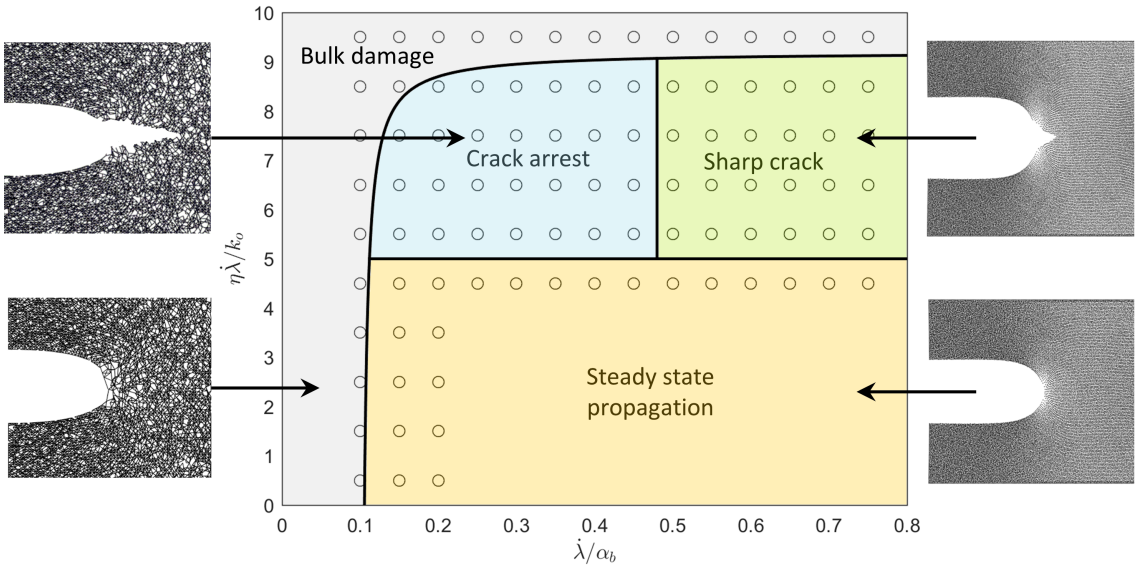

Figure 8: Effect of viscoelasticity, dynamic bond breakage, and stretch rate on the fracture patterns of polymer networks. The figures shows four different failure patterns: Crack blunting and bulk damage, steady state crack propagation, crack arrest, and non steady state crack propagation (sharp crack). An example of each failure pattern is shown in the figure.

The observed crack patterns are briefly summarized below. A more detailed investigation is reported elsewhere.

5.3.1 Crack blunting and bulk damage:

This pattern is reported for the cases where stretch rate, $\dot{\lambda}$ is too small compared to bond breakage rate, α_b, or the normalized viscous damping $\eta\dot{\lambda}/k_o$ is very high. In this pattern, the crack tip blunts and force concentration at the tip reduces, thus reducing the localized damage in the crack tip zone and allowing dynamic bond breakage to take place ahead of the crack tip and no crack propagation occurs as shown in Fig.8 lower left insert.

5.3.2 Steady state crack propagation:

This pattern is reported for cases with relatively small normalized polymer chain viscous damping $\eta\dot{\lambda}/k_o$ when the stretch rate $\dot{\lambda}$ to bond breakage rate α_b ratio is higher than the previous case. In this pattern, the crack initiates at the notch tip and propagates in a steady state manner, no significant bulk damage is observed. Since viscous damping is small, the polymer chains surrounding the crack quickly rebound to their reference length thus keeping the parabolic shape of the crack tip as shown in Fig.8 lower right insert.

5.3.3 Non-steady state crack propagation:

This pattern is reported when the normalized polymer chain viscous damping $\eta\dot{\lambda}/k_o$ is higher than the previous case and stretch rate $\dot{\lambda}$ to bond breakage rate α_b is relatively high. The crack initiates at the notch tip. However, due to the high viscoelasticity, two phenomena are observed: (i) the crack propagates slower than the steady state case, and (ii) the links around the crack tip only partially relax to a stretched configuration due to the viscous damper. This leads to the sharp crack profile where the crack surface is characterized by two parabolic shapes, a blunt one that belongs to the region of the initial notch and a sharp one for the new surface created by the propagating crack as shown in Fig.8 upper right insert. This sharp crack increases the force concentration at the tip thus increasing the crack speed and leading to non-steady state propagation. In extreme cases, a crack-inside-crack failure pattern is observed. These failure patterns have been reported in previous experimental work, e.g., [31].

5.3.4 Crack arrest:

This pattern is an intermediate case between case one (bulk damage) and case 3 (Non-steady state crack propagation). The crack initiates at low speed and starts propagation. However, the bulk damage accumulates at a rate faster than the crack propagation thus the crack stops propagating and bulk damage takes over. This is shown schematically in Fig.8 upper left insert.

We note that some of these crack patterns have been partially reported in prior theoretical investigations [32]. However, the phase diagram shown above representing the complete landscape of rate dependence effects, has not been reported before to the best of our knowledge.

6 Discussion

Fracture of polymer networks is a rate-dependent nonlinear problem in which macroscopic response depends on the details of network microstructure. In a previous study [22], we have introduced an adaptive model based on the Quasicontinuum approach for analyzing fracture in nonlinear elastic polymer networks. The proposed method starts from fundamental link scale mechanics and consistently computes macroscopic response but it was limited to elastic networks without any rate-dependence behavior. In the present work, we propose an extension to the method to account for different sources of rate-dependence in polymer networks such as viscoelasticity at the chain level and dynamic bond breakage.

This work aims to bring new innovations in both the application domain as well as the method formulation to the continuous development of the quasicontinuum approaches in modeling lattice materials. On the application level, this work brings the QC method into the discussion of modeling

fracture in rate-dependent polymeric and soft materials. On the method formulation, we have proposed homogenization rules for axially loaded lattices that account for both material and geometric nonlinearities in addition to viscoelastic behavior and nonlinear rate effects through dynamic bone breakage, and implemented these developments in a nonlinear finite element framework. Moreover, we have developed an adaptivity scheme that allows for transition between homogenized material and network chains where the refinement criteria depend not only on the deformation gradient, as has been done in earlier studies, but also on link damage properties. This is necessary, particularly for highly disordered networks, that allows triggering refinement and crack nucleation at the locations of weaker links in absence of a notch or a pre-existing crack.

The main advantage of the proposed QC framework is that it enables efficient modeling of large scale polymer networks without neglecting the effect of the microstructure and without assuming any critical macroscopic parameters such as fracture energy, or material length scale. Only local failure criteria at the chain level, that may be rigorously computed directly from explicit models of a single chain [25, 3, 33] is needed. Thus, the QC framework combines the advantages of continuum and discrete modeling of soft polymeric materials. The QC method requires much less run time, and memory than a full discrete model while providing higher accuracy and insights into the fracture process than the continuum approaches. Furthermore, the QC approach has the flexibility of adding small scale physics and topology, which makes it suitable for taking advantage of recent advances in experimental techniques.

Viscoelasticity and rate-dependent failure are critical feature in the mechanical response of polymeric materials such as rubber and gel. The proposed extension to the QC method allows incorporating rate-dependence in the polymer networks mechanical response. A homogenization rule is proposed to map the viscoelastic chain behavior from the microscale (network level) to the macroscale (QC level). Here, we have assumed that the polymer chain viscoelastic behavior follows a Kelvin-Voigt model, where each link consists of a nonlinear elastic spring that follows the worm-like chain model in parallel to a pure viscous damper with damping force that is a function of the link stretch rate. The same approach can be applied to more sophisticated viscosity models. The damping matrix is assembled then a predictor-corrector schemes is used to solve the resulting linearized quasi-dynamic system at each time step within the nonlinear finite element framework. This approach allows the emergence of viscoelasticity on the continuum scale.

Dynamic bond breakage is a source of nonlinear rate-dependence in polymer networks where the formation and breakage of bonds between the polymer and the cross-linking molecule depends on the force in the stretched polymer chain and the pulling rate [25, 3]. Here we consider dynamic bond breakage in the fully discrete zone and implement a mesh refinement criterion to refine continuum elements that contain a chain approaching breakage to fully discrete representation. This extension allows the QC approach to model transient polymer networks with reversible bonding and self healing. It may also be extended in a straight forward way to consider the hidden length mechanism [25, 34, 3, 35].

Automatic mesh adaptivity is a key aspect of QC approaches that leads to significant computational savings by reducing the initial fully resolved zone. However, as the crack propagates, the ratio of repnodes increases, especially in cases of highly non-uniform networks, leading to reduced computational savings. Here we modified the link stretch mesh refinement criterion to calculate the maximum principal stretch in each continuum element. This stretch is then compared to the maximum stretch threshold. It is also used to calculate the dynamic bond breakage parameter using Eq.20 to check the dynamic bond breakage refinement criterion. In addition, the same time adaptivity scheme discussed in Ghareeb and Elbanna [22] is utilized to balance accuracy of resolving crack propagation and computational savings.

Our results for fracture and damage of rate-dependent disordered networks suggest that stretch rates have significant effects on the network strength, toughness, and fracture patterns. For networks with viscoelasticity in the polymer chain behavior and link stretch based damage criterion, the network strength and toughness scale with the network stretch rate. For networks with dynamic bond breakage, the network strength and toughness have a logarithmic dependence on the stretch rate. The trade-off between viscous damping and dynamic bond breakage parameters has a direct effect on the damage and fracture pattern of polymer networks. Modeled networks were found to follow one of four failure patterns: Crack blunting followed by bulk damage, steady state crack propagation, crack arrest followed by bulk damage, and non steady state crack propagation

were sharp cracks and crack-in-crack patterns were observed. These results agree with and further extend previous theoretical studies [32]. The results also agree with recent experimental observations [31] of fracture of polymeric materials and provide insights on design of tough polymer networks through direct control of the microstructure characteristics. Furthermore, the results show that the QC method provides a flexible tool for reassessing polymer network micro scale physics at larger scales with less sensitivity to sample boundaries.

Modeling of the rate-dependent response of polymer networks with reversible bonding has been the focus of previous research studies. For example, Hui et al. [36] proposed a 3D finite strain constitutive model for self-healing gels by keeping track, in an aggregate way, of the time evolution of bond breakage and formation. Zhang et al [37] developed a coupled cohesive-zone and bulk viscoelasticity, idealized using Mullins-effect, model capable of describing fracture energies and strain fields around crack tips in soft materials under large deformation. Zhang et al. [38] investigated the hierarchical dynamics of a transient polymer network cross-linked by orthogonal dynamic bonds. Kothari et al. [3] studied the damage evolution and the force-displacement response of polymer networks for different loading rates, network topology, and cross-linking density. Our model is distinct from prior research work in several aspects. First, our model accounts for network topology around crack tips and areas of high interest while keeping the bulk viscoelastic effects, thus reducing the boundary effects on crack propagation. We also use transition state theory approach to model the bond dynamics which provides a direct link to bond-specific chemical characteristics and naturally account for nonlinear rate effects. Furthermore, the QC method does not impose any heuristic length scales or predetermined forms of macroscale cohesive laws or values of fracture energy. The effective response, including linear and nonlinear rate dependence, emerges naturally through linking the chain scale physics with topology, structure, and loading.

Extending the QC method to model rate-dependence in polymer networks, including dynamic bonds, could lead to efficient modeling of fatigue in soft materials. Evidence has accumulated that some soft materials, such as hydrogels, suffer fatigue under prolonged loads. Symptoms include change in properties, as well as nucleation and growth of cracks [39]. Recent studies showed that fatigue of soft materials depends on the details of the network topology and the polymer chains bond properties [39, 40]. Thus, using the multiscale capabilities of the QC method could lead to more insights into the problem. Further development of the QC method to include additional physics such as poroelasticity and self-healing of polymer chains cross-linkers, will enable this progress.

While rate-dependence and viscoelasticity are critical features in modeling soft polymeric materials, accurate modeling of the mechanical behavior of polymer networks may involve more physics beyond the elastic and viscoelastic interactions between polymer chains such as friction and entanglement.While it is possible to synthesize near ideal polymer networks, like the one considered in the current work, that are essentially free of entanglements [41, 42], incorporating these additional features may be important for a variety of applications and to emulate networks that are synthesized using more traditional techniques. The QC framework is flexible enough to incorporate these extensions and this will be further investigated in future work.

7 Conclusions

To summarize, the extended QC framework proposed in the current work enables significant insight into the role of microstructure on macroscopic rate-dependent fracture response in polymer networks. Both viscoelasticity in the polymer-chain constitutive relation and dynamic bond breakage are considered. This method is envisioned to lead to identification of fundamental processes controlling fracture patterns and toughness in a variety of networked materials, including polymer networks. It may also enable the discovery of new material designs with non-classical fracture response.

Our main conclusions are summarized as follows:

1. The extended QC approach enables modeling rate-dependent fracture in polymer networks in a way that combines advantages from both discrete and continuum approaches.

2. The extended QC method takes into consideration the viscoelasticity on the chain level in

addition to dynamic bond breakage.

3. Adaptivity allows the QC mesh to evolve as the damage initiates and grows, increasing accuracy and computational savings. Mesh refinement is triggered by link stretch damage, dynamic bond breakage, or nonuniformity in the deformation gradient.

4. Loading rate significantly affect the polymer network strength, toughness, and fracture patterns.

5. The trade-off between polymer chain viscoelasticity and dynamic bond breakage parameters controls the damage and fracture patterns of polymer networks.

A Appendix: Derivation of the homogenized viscoelastic stress tensor and the corresponding modulus

A.1 Micro-macro energy consistency condition:

We establish the micro-macro scale homogenization relation based on the Hill-Mandel condition [20, 21] for the viscous force in Eq.1. This condition requires the volume average of the variation of work on the micro level to be equal to the variation of local work on the macro level:

$$\delta W_{Macro} = \delta W_{micro} \tag{A.1}$$

In terms of macro deformation gradient tensor and the first Piola-Kirchhoff viscous stress tensor, the condition reads [43]:

$$\mathbf{P}^v_M : \delta \mathbf{F}_M = \frac{1}{V_o} \sum_{p=1}^{N_p} \left(\vec{f}^v_p . \delta \vec{l}_p \right) \tag{A.2}$$

Where $\vec{f}^v_p$ and $\vec{l}_p$ are the viscous force component and the length of each link in the current configuration, N_p is the number of links. Using $\delta \vec{l}_p = \vec{L}_p \delta \mathbf{F}^T$, where $\vec{L}_p$ is the link length in the original configuration, and using Voigt assumption (i.e the deformation gradient on the micro and macro scale is the same). The homogenized 1^{st} Piola-Kirchhoff viscous stress is given by:

$$\mathbf{P}^v_M = \frac{1}{V_o} \sum_{p=1}^{N_p} \left(\vec{f}^v_p \otimes \vec{L}_p \right) \tag{A.3}$$

Where the subscript M denotes the macro level tensors.

To calculate the tangent tensor required to update the viscous stress, we start by taking the variation of $\mathbf{P}^v_M$:

$$\delta \mathbf{P}^v_M = \frac{1}{V_o} \sum_{p=1}^{N_p} \left(\frac{\partial \vec{f}^v_p}{\partial \vec{V}_p} . \delta \vec{V}_p \right) \otimes \vec{L}_p \tag{A.4}$$

Where $\vec{V}_p$ is the stretch rate of the link. Substituting $\delta \vec{V}_p = \delta \dot{\mathbf{F}} \vec{L}_p$ and using Voigt assumption, the homogenized 4^{th} order viscosity tensor is given by:

$$\mathbf{C}^{P^v \dot{F}} = \frac{1}{V_o} \sum_{p=1}^{N_p} \left(\vec{L}_p \otimes \eta_p \otimes \vec{L}_p \right) \tag{A.5}$$

Where $\eta_p = \partial \vec{f}^v_p / \partial \vec{V}_p$ is the viscous damper parameter.

For increasing the computational efficiency, it is more convenient to use the objective symmetric 2^{nd} Piola-Kirchhoff viscous Stress tensor and the corresponding viscosity tensor. By definition, the 2^{nd} Piola-Kirchhoff Stress tensor is given by:

$$\mathbf{S}^v_M = \mathbf{F}^{-1}_M \mathbf{P}^v_M \tag{A.6}$$

Using indicial notation and substituting for $\mathbf{P}^v_M$ from Eq.A.3, then using Voigt assumption:

$$S^v_{ij} = \frac{1}{V_o} \sum_{p=1}^{N_p} \left({F_{ik}}^{-1} f^v_k L_j \right)_p \tag{A.7}$$

The subscript M is dropped for convenience. To derive the tensor relating the viscous PK2 tensor and the rate of the Green strain, we start by varying the relation between PK1 and PK2 and follow the derivation detailed in Ghareeb and Elbanna (2020) [22]. The homogenized 4^{th} order viscosity tensor is given by:

$$C^{S^v \dot{E}}_{ijkl} = \frac{1}{V_o} \sum_{p=1}^{N_p} \left(L_j F^{-1}_{im} \frac{\partial {f^v}_m}{\partial V_n} F^{-1}_{kn} L_l \right) - F^{-1}_{in} F^{-1}_{ln} S^v_{jk} \tag{A.8}$$

References

[1] C. Creton and M. Ciccotti, "Fracture and adhesion of soft materials: a review," *Reports on Progress in Physics*, vol. 79, p. 046601, 4 2016.

[2] R. Everaers and K. Kremer, "Topology effects in model polymer networks," *AIP Conference Proceedings*, vol. 615, no. April, pp. 615–626, 2009.

[3] K. Kothari, Y. Hu, S. Gupta, and A. Elbanna, "Mechanical Response of Two-Dimensional Polymer Networks: Role of Topology, Rate Dependence, and Damage Accumulation," *Journal of Applied Mechanics*, vol. 85, p. 031008, 1 2018.

[4] A. N. Gent, "A new constitutive relation for rubber," *Rubber Chemistry and Technology*, vol. 69, no. 1, pp. 59–61, 1996.

[5] R. S. Rivlin, "Large Elastic Deformations of Isotropic Materials. IV. Further Developments of the General Theory," *Philosophical Transactions of the Royal Society A: Mathematical, Physical and Engineering Sciences*, vol. 241, no. 835, pp. 379–397, 1948.

[6] E. M. Arruda and M. C. Boyce, "A three-dimensional constitutive model for the large stretch behavior of rubber elastic materials," *Journal of the Mechanics and Physics of Solids*, vol. 41, no. 2, pp. 389–412, 1993.

[7] Y. Hu, X. Zhao, J. J. Vlassak, and Z. Suo, "Using indentation to characterize the poroelasticity of gels," *Applied Physics Letters*, vol. 96, no. 12, pp. 8–11, 2010.

[8] S. A. Chester and L. Anand, "A thermo-mechanically coupled theory for fluid permeation in elastomeric materials: Application to thermally responsive gels," *Journal of the Mechanics and Physics of Solids*, vol. 59, no. 10, pp. 1978–2006, 2011.

[9] M. J. Buehler, *Atomistic modeling of materials failure*. Boston, MA: Springer US, 2008.

[10] C. P. Broedersz and F. C. Mackintosh, "Modeling semiflexible polymer networks," *Reviews of Modern Physics*, vol. 86, no. 3, pp. 995–1036, 2014.

[11] E. B. Tadmor, M. Ortiz, and R. Phillips, "Quasicontinuum analysis of defects in solids," *Philosophical Magazine A: Physics of Condensed Matter, Structure, Defects and Mechanical Properties*, vol. 73, no. 6, pp. 1529–1563, 1996.

[12] R. E. Miller and E. B. Tadmor, "The Quasicontinuum Method: Overview, applications and current directions," *Journal of Computer-Aided Materials Design*, vol. 9, pp. 203–239, 10 2002.

[13] V. B. Shenoy, R. Miller, E. B. Tadmor, D. Rodney, R. Phillips, and M. Ortiz, "An adaptive finite element approach to atomic-scale mechanics - The quasicontinuum method," *Journal of the Mechanics and Physics of Solids*, vol. 47, no. 3, pp. 611–642, 1999.

[14] A. Ghareeb and A. Elbanna, "An Adaptive Quasi-Continuum Approach for Modeling Fracture in Networked Materials: Application to Modeling of Polymer Networks," 2019.

[15] J. Li, Y. Hu, J. J. Vlassak, and Z. Suo, "Experimental determination of equations of state for ideal elastomeric gels," *Soft Matter*, vol. 8, no. 31, pp. 8121–8128, 2012.

[16] T. D. Nguyen, C. M. Yakacki, P. D. Brahmbhatt, and M. L. Chambers, "Modeling the relaxation mechanisms of amorphous shape memory polymers," *Advanced Materials*, vol. 22, no. 31, pp. 3411–3423, 2010.

[17] A. Kumar and O. Lopez-Pamies, "On the two-potential constitutive modeling of rubber viscoelastic materials," *Comptes Rendus - Mecanique*, vol. 344, no. 2, pp. 102–112, 2016.

[18] J. Zhang and M. Ostoja-Starzewski, "Mesoscale bounds in viscoelasticity of random composites," *Mechanics Research Communications*, vol. 68, pp. 98–104, 2015.

[19] J. Zhou, L. Jiang, and R. E. Khayat, "A micro–macro constitutive model for finite-deformation viscoelasticity of elastomers with nonlinear viscosity," *Journal of the Mechanics and Physics of Solids*, vol. 110, pp. 137–154, 2018.

[20] R. Hill, "Elastic properties of reinforced solids: Some theoretical principles," *Journal of the Mechanics and Physics of Solids*, vol. 11, no. 5, pp. 357–372, 1963.

[21] P. M. Suquet, "Local and global aspects in the mathematical theory of plasticity.," *In Plasticity Today: Modelling, Methods and Applications*, pp. 279–310, 1985.

[22] A. Ghareeb and A. Elbanna, "An adaptive quasicontinuum approach for modeling fracture in networked materials: Application to modeling of polymer networks," *Journal of the Mechanics and Physics of Solids*, vol. 137, p. 103819, 5 2020.

[23] J. F. Marko and E. D. Siggia, "Stretching DNA," *Macromolecules*, vol. 28, no. 26, pp. 8759–8770, 1995.

[24] J. F. Marko, "DNA under high tension: Overstretching, undertwisting, and relaxation dynamics," *Physical Review E - Statistical Physics, Plasmas, Fluids, and Related Interdisciplinary Topics*, vol. 57, no. 2, pp. 2134–2149, 1998.

[25] C. K. Lieou, A. E. Elbanna, and J. M. Carlson, "Sacrificial bonds and hidden length in biomaterials: A kinetic constitutive description of strength and toughness in bone," *Physical Review E - Statistical, Nonlinear, and Soft Matter Physics*, vol. 88, p. 12703, 7 2013.

[26] G. I. Bell, "Models for the specific adhesion of cells to cells," *Science*, vol. 200, no. 4342, pp. 618–627, 1978.

[27] L. A. Beex, R. H. Peerlings, and M. G. Geers, "A multiscale quasicontinuum method for dissipative lattice models and discrete networks," *Journal of the Mechanics and Physics of Solids*, vol. 64, no. 1, pp. 154–169, 2014.

[28] O. Rokoš, R. H. Peerlings, J. Zeman, and L. A. Beex, "An adaptive variational Quasicontinuum methodology for lattice networks with localized damage," *International Journal for Numerical Methods in Engineering*, vol. 112, no. 2, pp. 174–200, 2017.

[29] K. Mikeš and M. Jirásek, "Quasicontinuum method extended to irregular lattices," *Computers and Structures*, vol. 192, pp. 50–70, 2017.

[30] M.-C. C. Rivara, "New longest-edge algorithms for the refinement and/or improvement of unstructured triangulations," *International Journal for Numerical Methods in Engineering*, vol. 40, pp. 3313–3324, 9 1997.

[31] M. Liu, J. Guo, Z. Li, C. Y. Hui, and A. T. Zehnder, "Crack propagation in a PVA dual-crosslink hydrogel: Crack tip fields measured using digital image correlation," *Mechanics of Materials*, vol. 138, no. August, p. 103158, 2019.

[32] S. Arora, A. Shabbir, O. Hassager, C. Ligoure, and L. Ramos, "Brittle fracture of polymer transient networks," *arXiv*, vol. 1267, 2017.

[33] Y. Mao and L. Anand, "Fracture of Elastomeric Materials by Crosslink Failure," *Journal of Applied Mechanics*, vol. 85, no. 8, p. 081008, 2018.

[34] A. E. Elbanna and J. M. Carlson, "Dynamics of Polymer Molecules with Sacrificial Bond and Hidden Length Systems: Towards a Physically-Based Mesoscopic Constitutive Law," *PLoS ONE*, vol. 8, no. 4, pp. 1–10, 2013.

[35] G. E. Fantner, T. Hassenkam, J. H. Kindt, J. C. Weaver, H. Birkedal, L. Pechenik, J. A. Cutroni, G. A. Cidade, G. D. Stucky, D. E. Morse, and P. K. Hansma, "Sacrificial bonds and hidden length dissipate energy as mineralized fibrils separate during bone fracture," *Nature Materials*, vol. 4, no. 8, pp. 612–616, 2005.

[36] C. Y. Hui and R. Long, "A constitutive model for the large deformation of a self-healing gel," *Soft Matter*, vol. 8, no. 31, pp. 8209–8216, 2012.

[37] T. Zhang, S. Lin, H. Yuk, and X. Zhao, "Predicting fracture energies and crack-tip fields of soft tough materials," *Extreme Mechanics Letters*, vol. 4, pp. 1–8, 2015.

[38] R. Zhang, C. Zhang, Z. Yang, Q. Wu, P. Sun, and X. Wang, "Hierarchical Dynamics in a Transient Polymer Network Cross-Linked by Orthogonal Dynamic Bonds," *Macromolecules*, 2020.

[39] R. Bai, J. Yang, and Z. Suo, "Fatigue of hydrogels," *European Journal of Mechanics, A/Solids*, vol. 74, no. December 2018, pp. 337–370, 2019.

[40] R. Bai, Q. Yang, J. Tang, X. P. Morelle, J. Vlassak, and Z. Suo, "Fatigue fracture of tough hydrogels," *Extreme Mechanics Letters*, vol. 15, pp. 91–96, 2017.

[41] T. Sakai, T. Matsunaga, Y. Yamamoto, C. Ito, R. Yoshida, S. Suzuki, N. Sasaki, M. Shibayama, and U. I. Chung, "Design and fabrication of a high-strength hydrogel with ideally homogeneous network structure from tetrahedron-like macromonomers," *Macromolecules*, vol. 41, no. 14, pp. 5379–5384, 2008.

[42] T. Sakai, Y. Akagi, T. Matsunaga, M. Kurakazu, U. I. Chung, and M. Shibayama, "Highly elastic and deformable hydrogel formed from tetra-arm polymers," *Macromolecular Rapid Communications*, vol. 31, no. 22, pp. 1954–1959, 2010.

[43] M. G. D. Geers, V. G. Kouznetsova, K. Matouš, and J. Yvonnet, "Homogenization Methods and Multiscale Modeling: Nonlinear Problems," in *Encyclopedia of Computational Mechanics Second Edition*, pp. 1–34, Chichester, UK: John Wiley & Sons, Ltd, 7 2017.